THE ASTRONOMICAL JOURNAL VOLUME 89, NUMBER 1 JANUARY 1984

AUTOMATED STAR COUNTS IN THE SOUTHERN GLOBULAR CLUSTER NGC 6809 (M55)

MICHAEL J. IRWIN
Institute of Astronomy, Madingley Road, Cambridge CB3 0HA, England

VIRGINIA TRIMBLE
Department of Physics, University of California, Irvine, California 92717
and Astronomy Program, University of Maryland, College Park, Maryland 20742

Received 6 June 1983; revised 23 September 1983

ABSTRACT

We report star counts, as a function of position and apparent magnitude, in the rich, relatively open southern globular cluster NGC 6809 (M55). Three AAO 150″ plates were scanned by the Automatic Plate Measuring System (APM) at the Institute of Astronomy, Cambridge, and 20 825 images were counted by its associated software. Previously known features of rich globular clusters which appear in the raw counts include a flattening of the luminosity function below $M_B \sim +5.2$, increased central concentration of bright stars relative to faint ones (normally interpreted as mass segregation), and mild deviations in radial profile from King models. Crowding of the field, which causes the counting procedure to miss faint stars preferentially near the cluster center, contributes to all of these, and may be responsible for all of the apparent mass segregation, but not for all of the other two effects. The deviations from a smooth radial profile are real in the sense of showing up in other counts of this and other clusters and are of marginal statistical significance (1–2σ for a Poisson distribution). The luminosity function is the most detailed so far published for a globular cluster, and its precise shape near main-sequence turnoff may be usable as an age indicator. Automated subtraction and comparison of plate pairs rediscovered five of the six known RR Lyrae variables and found one additional candidate variable of about the same brightness, as well as eight possible variables near the faint limit of the scans. Three of these are confirmed as variable by Liller, using conventional techniques. These are of appropriate luminosity, periods, and number to be either W UMa (contact binary) or BY Dra (spotted, rotating) stars and so are deserving of further investigation. We conclude that the APM in its normal image analysis mode did at least as well in its first try at measuring stars in a crowded globular cluster field as a novice human observer would. An experienced human observer can, however, extract more reliable information in the centers of such clusters, and the APM software can probably be modified to imitate some of the fruits of such experience.

I. INTRODUCING THE APM

Counting stars as a function of apparent brightness and position in the sky has been part of astronomy at least since the time of Newton (1962; Hoskin 1982). Star counts, properly done, can be remarkably informative, yielding information on problems ranging from the overall structure of our galaxy (Herschel 1785; Bahcall and Soneira 1981) to the detailed distribution of obscuring matter (Bok 1977; Tomita *et al.* 1979; Trimble 1977). They can also be remarkably tedious to perform (Weistrop 1968), requiring great patience and great consistency on the part of the counter. This is particularly so for the crowded fields of globular clusters, where star counts remain a major source of information on cluster structure and dynamics (King *et al.* 1968; Harris and Racine 1979).

Interesting points not yet fully clarified include the Initial Mass Function of the main-sequence stars, the extent of mass segregation within clusters, deviations of the radial profiles from classic King (1966) models, and the differences in these things from one cluster to another. Da Costa (1982) and others have begun to address these questions with star counts done by traditional methods. We here ask the additional question: can we be replaced by a machine? The answer, perhaps predictably, proves to be a qualified yes. Herzog and Illingworth (1977) reached a similar conclusion using a PDS scanner and a CDC 6400 computer, but their counts do not seem to have been published.

The machine in our case is the Automatic Plate Measuring System (APM) at the Institute of Astronomy in Cambridge (Kibblewhite *et al.* 1983). It is the product of nearly a decade of SERC-sponsored development (under the leadership of Edward Kibblewhite) and came into regular use in 1980. Its distinctive features include a laser spot scanner, permitting very rapid scanning and low measurement noise, and on-line processing capability that includes provision for density wedge calibration, sky background estimation, noise removal, and automatic image detection and computation of image parameters (integrated isophotal intensities, positions, second order moments, peak intensities, and areal profiles).

The high scanning speed of the APM enables us to take extra care in determining the sky background. All measurements are done in two passes. On the first pass, the sky background is estimated. The plate is partitioned into roughly $\frac{1}{2}\times\frac{1}{2}$-mm pixels, and, for each of these background pixels, an array of 64×64 intensity measurements is made. The interpolated mode of this array is used as an initial estimate of the sky background. When the full $2D$ array of initial background intensity measurements has been made, it is further processed through a nonlinear filter to give the final background values. The purpose of the filter is to detect and correct background values contaminated by the presence of resolved astronomical images and to smooth the final values. By making use of all the background information in this way, it is possible to estimate local background levels over extended objects such as globular clusters or nearby large galaxies.

On the second pass over the plate, a threshold is defined as a fixed additive isophote above the sky background, and

 0004-6256/84/010083-12$00.90

areas of connected pixels above threshold (i.e., images) are detected and parametrized on line.

The parameters of each detected image are recorded and stored on magnetic tape for subsequent off-line analysis. In this way, the enormous amount of potential information stored on a photographic plate (4 billion bytes for a typical $14 \times 14''$ Schmidt survey plate) is reduced to manageable proportions with little loss of genuine information about the real astronomical images.

Each plate measured on the APM is aligned with respect to a standard catalog of stars (SAO or PERTH 70), permitting direct conversion of machine coordinates to right ascension and declination with a typical accuracy of $1''$. This should not be confused with the intrinsic positional accuracy of the APM which is better than $0''.1$ when sufficiently accurate reference stars are used to define the coordinate transformation. Inverting the alignment procedure, the machine can return to a given RA and δ on a previously scanned plate and generate pixel intensity maps or other detailed information for candidate variables, fields around radio source positions, or other interesting objects.

Finally, a technique has been developed for establishing an internal magnitude scale for stellar objects that is linearly related to real apparent magnitude over a dynamic range stretching from the plate limit to the brightest stars in a field (Bunclark and Irwin 1983). By making use of the largely uniform sensitivity of photographic plates, the calibration problem can be reduced to one of finding a single, nonlinear transformation that maps, in this case, isophotal magnitudes into linear magnitudes. Since we have, *a priori*, identically shaped stellar images distributed over the plate, there must be sufficient information already present to define the system response without the need for calibration spots. Areal profiles (e.g., de Voucouleurs 1948) provide a simple and reliable measure of the image shape which is well suited to investigating the system response using large numbers of images. By requiring that the areal profile of a star be independent of its magnitude, we can then derive a magnitude index for stellar images that is linearly related to photoelectric magnitudes with no loss of accuracy relative to the isophotal intensities. This permits considerable extrapolation of whatever magnitude sequences may already have been established in the field.

Measurements of fields including the South Galactic Pole and M31 where faint photoelectric sequences exist have thoroughly tested the method. It has been used here to extend the stellar sequences of Alcaino (1975), Harris (1975), and Lee (1977) down to $J = 21.0$. The APM has also numerous other capabilities (e.g., in processing and classification of extended images) not required for this project. A manual describing its operation in more detail is available on request from MJI.

II. TECHNICAL DETAILS

a) The Plates and Scans

Our original purpose, inspired by a suggestion from Ivan King to VT, was a last-ditch effort to find, or rule out, relatively unevolved binaries in a globular cluster by searching for W UMa variables well down on the main sequence (cf. Webbink 1980 and Trimble 1980 for reviews of this ancient problem). David Hanes and David Malin took three well-matched plates of M55 on three successive evenings in late 1981 on the $150''$ telescope at the Anglo-Australian Observatory. The plates are IIIa-J's, exposed through a GG 385 filter (photographic J band), and cover a usable area of $30 \times 32.5'$ approximately centered on the cluster. They therefore reach the nominal tidal radius of the cluster, $18.6'$ (Peterson and King 1975; Peterson 1976), only at the corners. These plates were scanned on the APM and the data analysis done on the Starlink VAX 11/780 at Cambridge using standard APM software.

In order to look for variables (Sec. V below), the APM necessarily generated for each plate a complete file of image intensities and positions down to a preselected threshold at about 20% above the sky background, corresponding to a limit of $B \sim 21.3$ or $M_B \sim +7.6$ for stars at the cluster distance, using Alcaino's (1975) value of $(m - M)_B^{\rm app} = 13.73$. The chosen threshold was a compromise between the desire for a faint limiting magnitude and the need to avoid large numbers of overlapping images. It is well above the plate limit, and our counts could probably, therefore, be pushed 1–$2^{\rm m}$ fainter in the outer parts of the cluster.

The data files list image brightness in an internal magnitude system, *APM*, ranging from 17.7 for the brightest stars in the field to 8.1 at threshold. The linearization procedure described above, normalized to the photoelectric sequences of Alcaino (1975), Harris (1975), and Lee (1977), yielded the transformation equations:

$$B = 28.73 - 0.948APM + 0.17(B - V), \quad (1)$$

$$J = 28.73 - 0.948APM. \quad (2)$$

Once these data files were assembled, it seemed a shame to waste them. Thus, out of curiosity, we used the numbers from the best plate to generate histograms of numbers of star images as a function of position and APM magnitude for the plate as a whole and for various subsets binned by apparent magnitude and by distance from the cluster center. The histograms looked enough like previously published star counts for the cluster to inspire further investigation.

b) Corrections for Background Stars

For most globular clusters, no reasonably deep plate is anywhere unpolluted. The main pollutants are images that overlap (called crowding or confusion) in the cluster core and background (really mostly foreground) stars that cease to be a negligible fraction of cluster stars in the outskirts (King *et al.* 1968). Only the latter can be dealt with in the traditional way here.

The surface density and luminosity function of background stars are, ideally, determined from a large region of sky adjacent to, but outside, the cluster of interest. Our plates are not quite large enough to permit this. The background luminosity function used (Figs. 1 and 2) represents the 1968 images outside $R = 15'.2$ (about eight times the core radius of $1'.74$, but less than the tidal radius of $18'.6$; Peterson and King 1975). The contamination by cluster stars should be $\lesssim 5\%$. The total surface density of background images, 6.81 per square minute, comes also from the corners of the plate (the right-hand side of Fig. 5, which shows images per unit area as a function of position). Examination of these images shows that the contribution from background galaxies is small, 0.69 per square minute for this limiting magnitude, leaving 6.12 star images per square minute. This is consistent with the number expected in this part of the sky down to $B = +21$, according to the models of Bahcall and Soneira (1981) and with extrapolations of the background density of brighter stars found for this cluster by King *et al.* (1968).

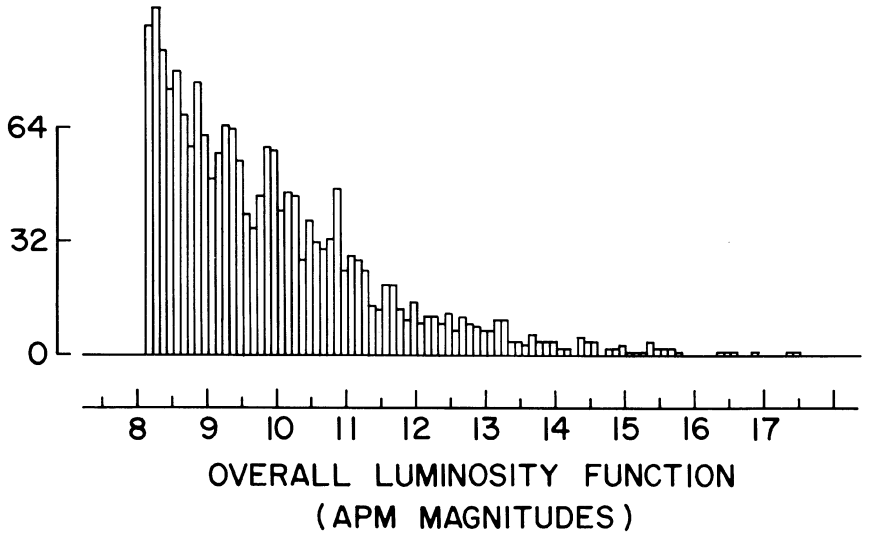

FIG. 1. Background luminosity function for M55 determined from 1968 images outside $R = 15.2'$. Numbers are total numbers of images (90% stars, 10% galaxies) in each bin 0.1 *APM* magnitude wide, not corrected or smoothed in any way. The function has considerable statistical noise, especially at the bright end, owing to the small plate area available for background determination.

Because the galaxy contribution is small and because we do not expect it to vary over the area of the cluster, we have simply subtracted the total background image luminosity function in the following analysis. The APM does, however, have the ability to distinguish star and galaxy images with considerable reliability.

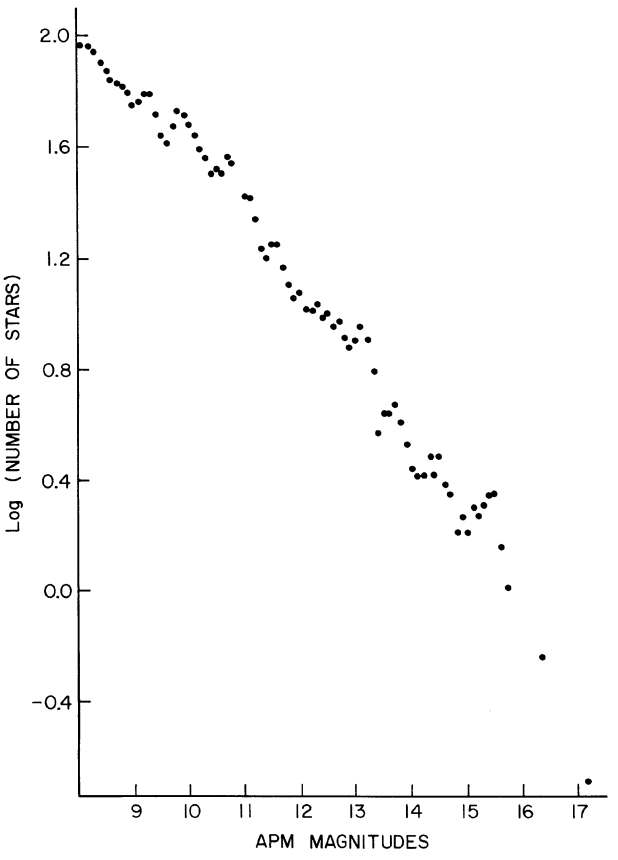

FIG. 2. Background luminosity function, slightly smoothed, as used to analyze counts in the cluster. The residual statistical noise is sometimes reflected in the counts in Figs. 3 and 4. The magnitude range $APM = 8$–17.2 is equivalent to $J = 21.1$–12.4. Numbers are total numbers of images in bins 0.1 *APM* wide over the 263 sq min available for background determination.

c) Corrections for Image Crowding

The standard algorithm for image crowding corrections (King *et al.* 1968) was derived empirically from counts done by experienced human observers on plates with a range of limiting magnitudes. It raises the logarithm of the number of stars counted per square minute, $\log f$, by an increment, δ, proportional to the log of the fraction of plate area covered by stellar images:

$$\delta = 0.429(\log fA + 1.735) + 0.15 \log(S/67.1), \quad (3)$$

where A is the area (in square minutes) of a typical image. The second term represents effects of scale difference between Palomar Schmidt plates (67".1/mm) and those used (16".24/mm for the AAT). Equation (3) says that crowding begins to cause one to miss stars when about 2% of the plate area is covered and that one misses 0.3 dex of stars for every additional dex of real images beyond that. The value of A must be estimated by the counter, and is probably the largest uncertainty in the application of Eq. (3) (King *et al.* 1968). Because human observers look at some complex combination of image intensities and shapes, A increases more slowly with star brightness than does isophotal area, and tends to be about the size of the seeing disc for all but the brightest images on a plate.

The APM analysis of a photographic plate proceeds rather differently, by estimating the local sky background and then setting a fixed isophote relative to this background above which to search for images. An image is defined as a region of simply connected pixels above the threshold isophote. Consequently, the area of a detached image is precisely defined and the probability of missing a star depends directly on the (readily calculable) probability of images overlapping.

To first order, therefore, the crowding corrections depend only on the average image size at the limiting isophote and on the local number density of stars. There will, of course, be second order effects involving the actual luminosity function, which, in turn, will perturb the measured luminosity function. These second order effects are complex to analyze and will be ignored here. That they will, however, introduce

some systematic error into the counts can be seen immediately by considering the case of a faint star whose image falls on the edge of the image of a brighter one. Being simply connected, the two will get counted as a single star; and the measured luminosity function will differ from the real one in having lost a faint star and in having a bright one get counted as brighter than it really is. This effect obviously flattens the measured luminosity function, and its neglect is the major uncertainty in the results presented in Secs. III and IV.

Let us call the average image area (in square minutes) A'. Then, as is shown in the Appendix, the relation between the observed number density, f, and the actual number density, f', is

$$f'A' \simeq -\tfrac{1}{4}\ln(1 - 4fA'). \quad (4)$$

Expanding the logarithm gives

$$f'A' \simeq fA'(1 + 2fA' + (16/3)f^2A'^2\cdots), \quad (5)$$

which emphasizes the strong dependence of the correction on average image size, A', and hence on the choice of threshold isophote.

Although Eqs. (3) and (4) are different in form, they lead to comparable corrections provided that A and A' are appropriately specified. A typical machine measurement results in an average image size a few times larger than that adduced by a human observer. Table I compares the two crowding corrections when the ratio $A/A' = 3$, the ratio of average image area set by the APM to that measured independently by VT. It is worth stressing that the table is meant only as a guide, since the two forms of correction are not, in general, strictly comparable. The automatic crowding correction defined by Eq. (4) is used throughout the remainder of the paper.

From the table, it is clear that: (1) Simple machine estimates of number density always require nonzero adjustments to be made, even for relatively low count levels. In contrast, a human observer, making use of all the image profile information, is rarely confused in these regions, and (2) for a high number density, isophotal analysis breaks down completely, because the majority of images are joined together at the threshold level. A human observer can still extract fairly reliable information in such fields, at least for the brighter stars, by ignoring the small images in and around the big ones.

The first point is largely compensated by the fact that the machine analysis is completely uniform, objective, and untiring over the field, so that the crowding correction is unambiguous. The machine analysis is also very fast at both image detection and luminosity assignment: typical AAT plates like these are aligned and measured in about 3 hr and the data processed in about 1 hr.

Dealing with the second point, so that faint stars whose images wholly or partially overlap the isophotal areas of brighter ones still get counted properly, will require a more sophisticated method of automatically analyzing crowded fields and a redefinition of what gets counted as an image. Many authors have suggested ways of dealing with moderately crowded fields, and we are currently developing an approach based on the ideas discussed by Newell (1979). It should be capable of coping with number densities up to 200 per sq min. This will permit automatic searches for variable stars nearly into the cluster center and the generation of reliable color-magnitude diagrams as a function of cluster radius. It will be used in future work on this and other clusters. We were, however, reluctant to abandon the simple (= quick and cheap) isophotal method until its potential and limitations had been fully explored. Meanwhile, the data on radial density distributions in Sec. IV are presented both uncorrected and with crowding corrections derived from Eq. (4).

TABLE I. A comparison of the crowding correction from King *et al.* [1968; Eq. (3)] with one appropriate for machine measurement [Eq. (4)].

fA'[a]	$\delta = \log_{10}(f'A'/fA')$[b]	$\delta = \log_{10}(f'A''/fA'') - 0.09$[c]
0.01	0.009	0.000
0.02	0.018	0.000
0.05	0.048	0.000
0.07	0.069	0.000
0.10	0.106	0.019
0.15	0.184	0.094
0.20	0.304	0.147
0.25	∞	0.189

[a] Fraction of plate covered with images of average area A' and number density f.
[b] Crowding correction for APM data.
[c] Crowding correction from King *et al.* (1968) algorithm but with image area A'' one-third that of APM isophotal image area (7.88 sq sec in these counts).

III. THE LUMINOSITY FUNCTION

Figures 3 and 4 present the measured luminosity function for the cluster as a whole and for inner and outer zones separately. The histograms (Fig. 3) come directly from the APM and have not been corrected for anything. The bin width, 0.1 *APM*, was chosen on the basis of the typical measurement accuracy, about 0.05 *APM*. Adding up all the radial zone histograms gives back precisely the total one.

The histogram of Fig. 3(a) is the most detailed luminosity function so far published for a globular cluster. A conspicuous feature is a rather sudden change in slope near $APM = 12.5$ ($M_J = 3.15$) where stars, turning off from the main sequence, begin to evolve rapidly. Paczyński (1983) suggests that the details of this slope change can be used as a cluster age indicator which, unlike evolutionary tracks in an HR diagram, will be largely free of difficulties introduced by the mixing length formalism. The histogram is, conspicuously, not smooth, though it could be made so by summing over bins as wide as those used in most previously published luminosity functions (e.g., Simoda and Tanikawa 1972). When similar data become available for other clusters, it will be worth looking for previously unknown, fine-scale features that may tell us something about the Initial Mass Function or changes in rate of stellar evolution.

The logarithmic differential luminosity functions (Fig. 4) have had appropriate amounts of background luminosity function (Figs. 1 and 2) subtracted and have been smoothed at the faint end by taking running means of three bins at a time and at the bright end by taking running means of as many bins as needed (5–8) to keep the net number of stars from going negative anywhere.

The whole-cluster luminosity function [Fig. 4(a)] shows the features one expects: a blip of horizontal branch stars at $APM = 16.1$ ($M_J = -0.2$), followed by a subgiant dip at $APM = 15.75$ ($M_J = +0.1$), and noticeable flattening below $APM = 10.5$ ($M_J = +5$). The ripple structure between $APM = 8$ and 10 is a reflection of the background luminosity function (Fig. 2) that was subtracted and tells us only that one really wants more than 1968 stars from which to determine this function! A related problem shows up at the bright end of the luminosity function. Because there happen to be

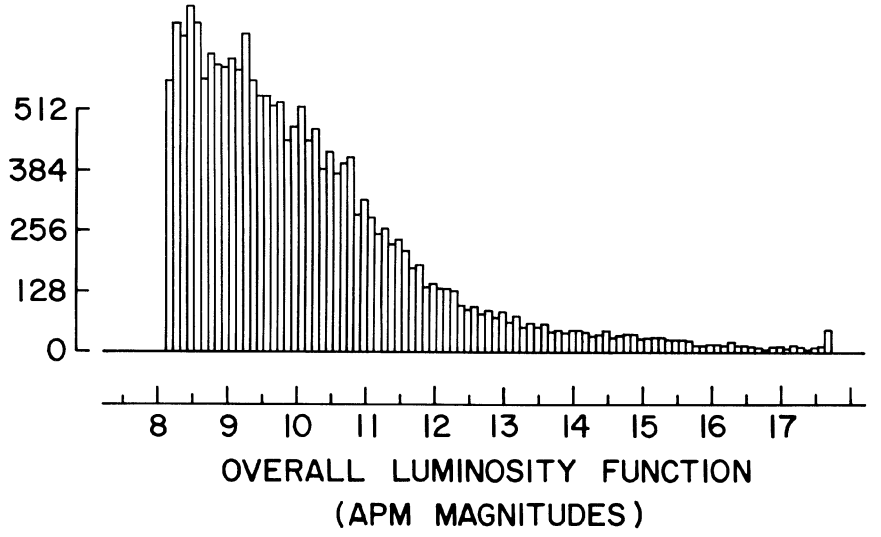

FIG. 3(a). Luminosity function for the entire cluster precisely as determined by the APM and not corrected for anything. 19 875 images are represented in bins 0.1 *APM* wide. The highest bin contains 698 images. The peak at APM = 17.6 represents clusters of star images in crowded areas of the plate perceived by the machine algorithm as single images. These are omitted from the luminosity functions graphed in Fig. 4. The change in slope near *APM* = 12.5 can perhaps be used as an age indicator for the cluster.

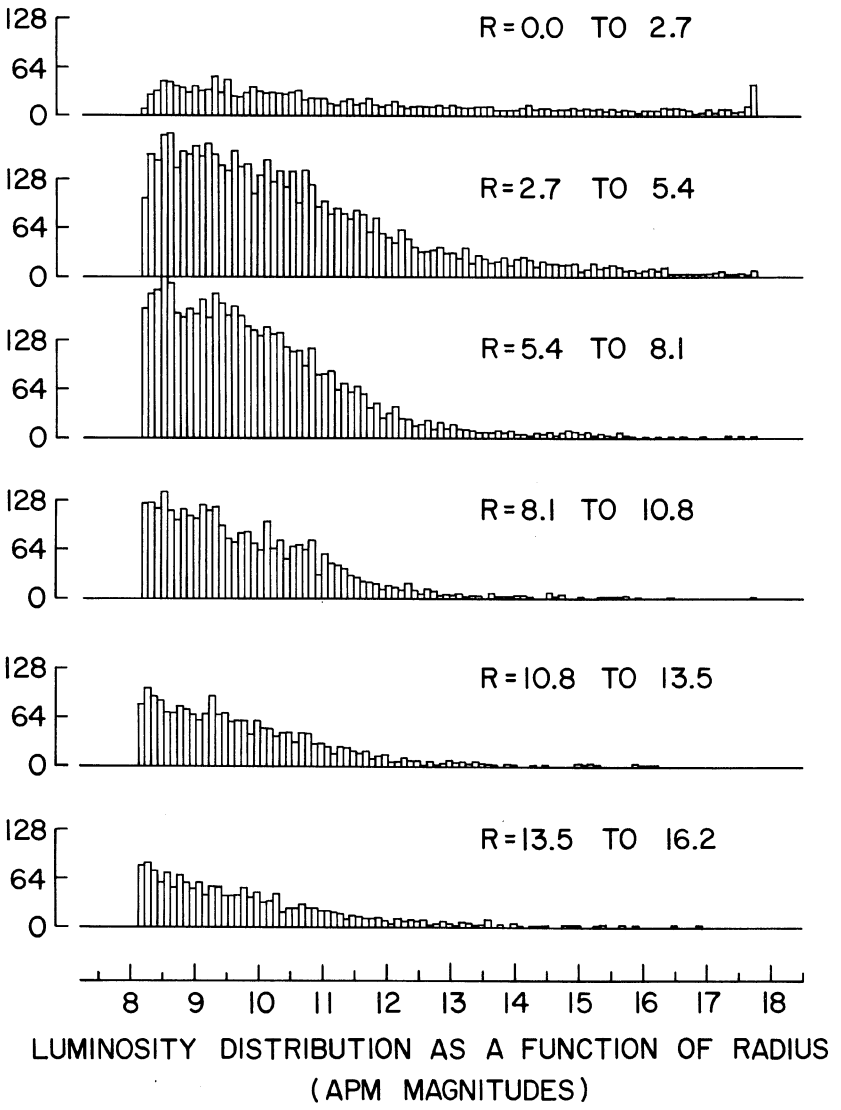

FIG. 3(b). Luminosity functions for radial zones of the cluster, from center to outskirts, precisely as determined by the APM. These six histograms summed give back Fig. 3(a). Notice that the artificial images brighter than *APM* = 17.5 are confined to the central, crowded zones. Many other effects of image crowding are also visible. Radii in minutes of arc.

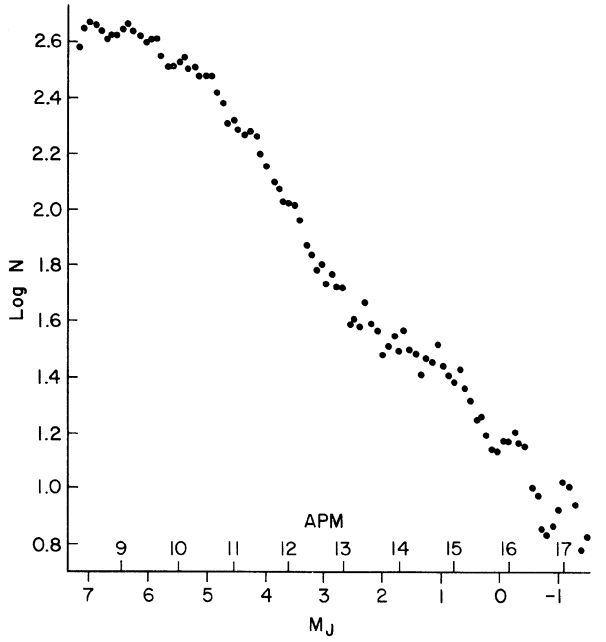

FIG. 4(a). Logarithmic luminosity function for the cluster as a whole after subtraction of appropriate background luminosity function and smoothing by running means of bins taken three at a time. Presumably real features include the horizontal branch near $M_J = 0$, followed by a subgiant dip, and gradual flattening below $M_J = 5$. The apparent excess of giants near $M_J = -1$ ($APM = 17$) is an artifact of the poor representation of that apparent brightness range in our background luminosity function.

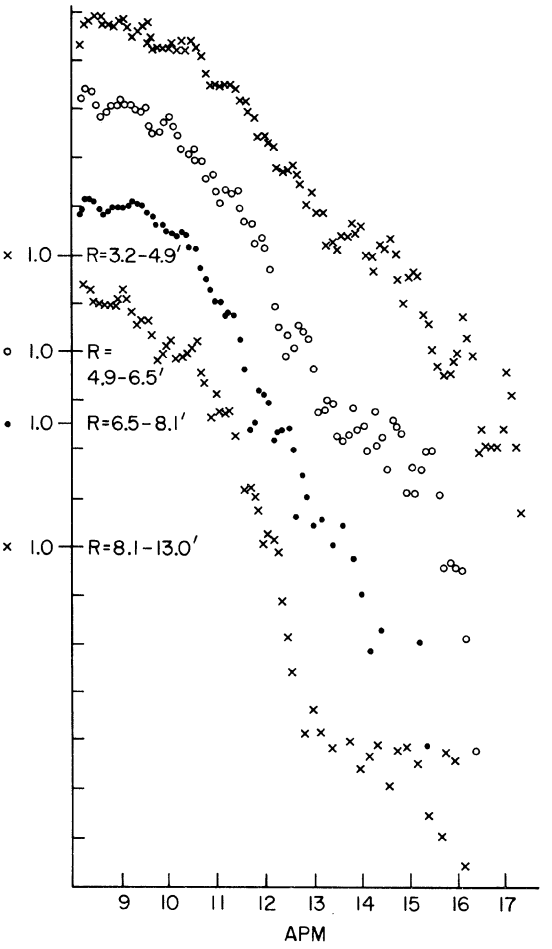

FIG. 4(b). Logarithmic luminosity function for radial zones of the cluster after subtraction of appropriate amounts of background luminosity function and smoothing by running means. Most of the differences among zones reflect the effects of image crowding on the way the APM identifies images and determines their brightnesses, which results in preferential missing of faint stars and enhancement of the brightness of bright ones, both effects increasing with increasing crowdedness. Section III addresses the possibility of residual real effects due to mass segregation, which could render the outer zones genuinely richer in faint stars. The four distributions are arbitrarily offset, the level at which $\log N = 1.0$ being indicated for each on the vertical axis. Tick marks are 0.2 dex apart.

only three background stars brighter than $APM = 16.5$ ($J = 13.1$; $M_J = -0.6$ at the distance of the cluster), the cluster appears artificially rich in giants. When allowance is made for these two problems introduced by inadequate background sampling, the cluster luminosity function falls well within the range of those found for other clusters (Da Costa 1982).

Comparison of the luminosity functions determined separately for inner and outer parts of the cluster leads to a less succinct conclusion. Suppose, for instance, we force the $APM = 13.5$–15.5 ($M_J = 0.3$–2.2) parts to coincide for all subsamples. Then, relative to the outermost ($R = 8.1$–$13'$) zone, all others are gravely deficient in $M_J \sim +7$ stars, by factors of 0.30 dex for $R = 6.5$–$8.1'$, 0.46 dex for $R = 4.6$–$6.5'$, 0.94 dex for $R = 3.2$–$4.9'$, and 0.70 dex for the cluster as a whole. The derivation of Eq. (4) explicitly ignored luminosity dependence, but if we assume that the dominant brightness-dependent effect is the loss of stars in proportion to the fraction of plate area covered by images of equal or greater brightness, then crowding corrections reduce these discrepancies to 0.15, 0.17, and 0.42 dex for the three inner zones and 0.35 dex for the cluster as a whole.

These discrepancies can have two causes: (1) mass (luminosity) segregation within the cluster, and (2) crowding-induced errors in the counts considerably in excess of naive predictions. In a cluster with great central condensation (i.e., large ratio of tidal to core radius), the former would not be implausible, as shown in Table II, which compares our apparent gradient in luminosity function with Da Costa's (1982) measurements for 47 Tuc and Da Costa and Freeman's (1976) model for M3. But, according to King (1975), mass segregation should not have progressed this far in so open and unrelaxed a cluster as M55 ($\log R_t/R_c = 1.03$ vs 1.96 for M15 and 2.03 for 47 Tuc; Harris and Racine 1979). Thus, the gradient is probably largely an artifact of luminosity-dependent confusion in the counts. In order to identify real mass segregation effects in relatively open clusters using automatic counts, it will be necessary either to calibrate the luminosity effects using plates with a range of limiting magnitudes or to improve the counting techniques along the lines suggested at the end of Sec. II.

IV. THE RADIAL PROFILE

Figures 5 and 6 show the radial profiles (numbers of stars per unit area as a function of radius) for the cluster as a whole and for bright and faint stars separately. As in the case of the luminosity function, the histograms come directly from the APM and have not been corrected for anything. The bins are 7.″6 wide. The graphs of Fig. 6 show, as dots, the profiles with appropriate amounts of background luminosity function subtracted and moderate smoothing [over three bins toward the cluster center and over enough bins (5–8) to keep the net number of stars positive in the cluster outskirts], and, as crosses, the same data, corrected first for crowding in accordance with Eq. (4), then for background stars, and finally smoothed. The crowding corrections for the cluster as a whole use Eq. (4) directly. Those for the subsets by brightness make a crude attempt to include luminosity effects by assuming that stars are lost from the counts in proportion to the fraction of the plate, fA', covered by images of equal or greater brightness to the ones being considered.

The total radial profile [Figs. 5(a) and 6(a)] presents no major surprises. It is well fit by a King (1966) model having $\log R_t/R_c = 1.0$ and $\log R_t = 1.3$ (Peterson and King give 1.03 and 1.27), apart from the small blip just outside $\log r = 0.7$ and the disappearance of the cluster star counts into the background at a radius about 1′ smaller than would be expected. Possibly our (not very well-determined) background density is a bit too high. Using 6.34 images per sq min (vs 6.81 adopted) would put the last measured point back onto the model curve.

The blip shows up in most of the subsamples by brightness and in the counts by King *et al.* (1968). It appears to be a real feature of the cluster. The actual number of images counted per 7.″61 radius bin in this zone ranges from 290 to 340, and the blip contains 45 "extra" images out of 956 counted ($N^{1/2} = 31$). It is, therefore a 1.5σ effect, assuming Poisson statistics, and so of marginal significance. King (1983) reports that the central regions of a number of other clusters, counted by conventional techniques, show similar features of similarly doubtful significance. It would be worth looking for correlations of their position and amplitude with other features of the clusters, on the off chance that they might have some interesting interpretation, like the secondary maxima suggested by Bahcall (1977) in clusters of galaxies.

Comparison of the radial profiles for stars classified by apparent brightness recreates the effect found in Sec. III: if we force the raw counts for all samples to coincide (apart from a zero-point shift in total numbers) in the outer parts of the cluster, then there is an apparent deficiency of faint stars everywhere inside $R = 8'$, the discrepancy rising to a factor of 4.3 for the faintest stars ($M_J > 6.3$) relative to the brighter ones ($M_J < 4.7$) at $R = 4'$. Again, as for the luminosity function, the difference is reduced but not eliminated by the crowding corrections, still becoming perceptible inside $R = 6.5'$ and dissolving into chaos inside 4′. As before, effects of this type and size would not be unreasonable for mass segregation in a very centrally condensed, relaxed cluster. But in this case, they are, we believe, due largely to luminosity dependence of crowding effects and the total breakdown of the machine algorithm when plate coverage approaches

TABLE II. Effects of mass segregation in globular clusters.

Cluster	R^{inner} (′)	$\frac{R^{\text{in}}}{R_{\text{tidal}}}$	$\log\left(\frac{N(\text{MS})}{N(\text{RG})}\right)^{a}$ (inner)	R^{outer} (′)	$\frac{R^{\text{out}}}{R_{\text{tidal}}}$	$\log\left(\frac{N(\text{MS})}{N(\text{RG})}\right)$ (outer)	$\frac{\Delta \log\left(\frac{N(\text{MS})}{N(\text{RG})}\right)}{\Delta \log(R/R_t)}$
47 Tuc[b]	14.0	0.32	0.00	24.0	0.55	+0.25	1.09
M3[c]	3.34	0.16	1.09	8.36	0.40	1.27	0.45
M55[d]	4.14	0.22	0.66	11.47	0.62	0.98	0.73

[a] Arbitrary normalization.
[b] Counts from Da Costa (1982).
[c] Model from Da Costa and Freeman (1976).
[d] Counts from this work.

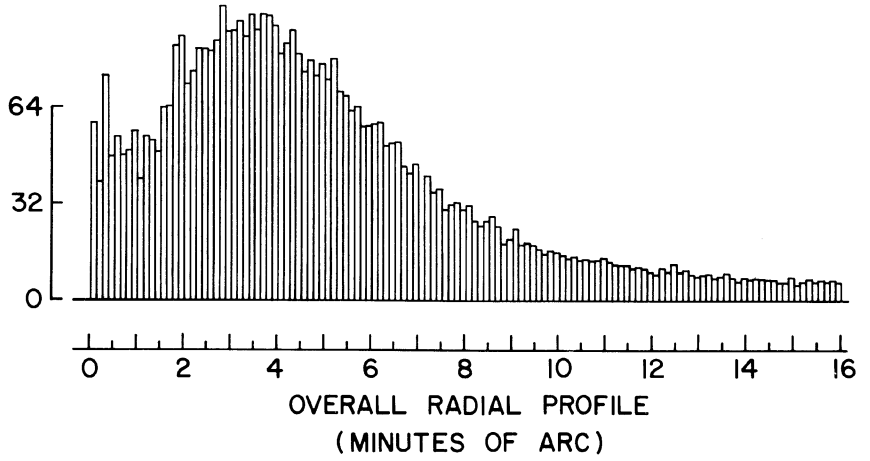

FIG. 5(a). Radial profile for the cluster as a whole, including all images identified by the APM. Numbers represent total numbers of stars per square minute in radial bins of 7.″61 (128 bins covering 16.2′). An apparent peak of about 100 stars per square minute is reached at $R = 3$–4′, inside which the real number density of stars continues to rise, but crowding results in the APM seeing fewer and fewer of the stars as separate images.

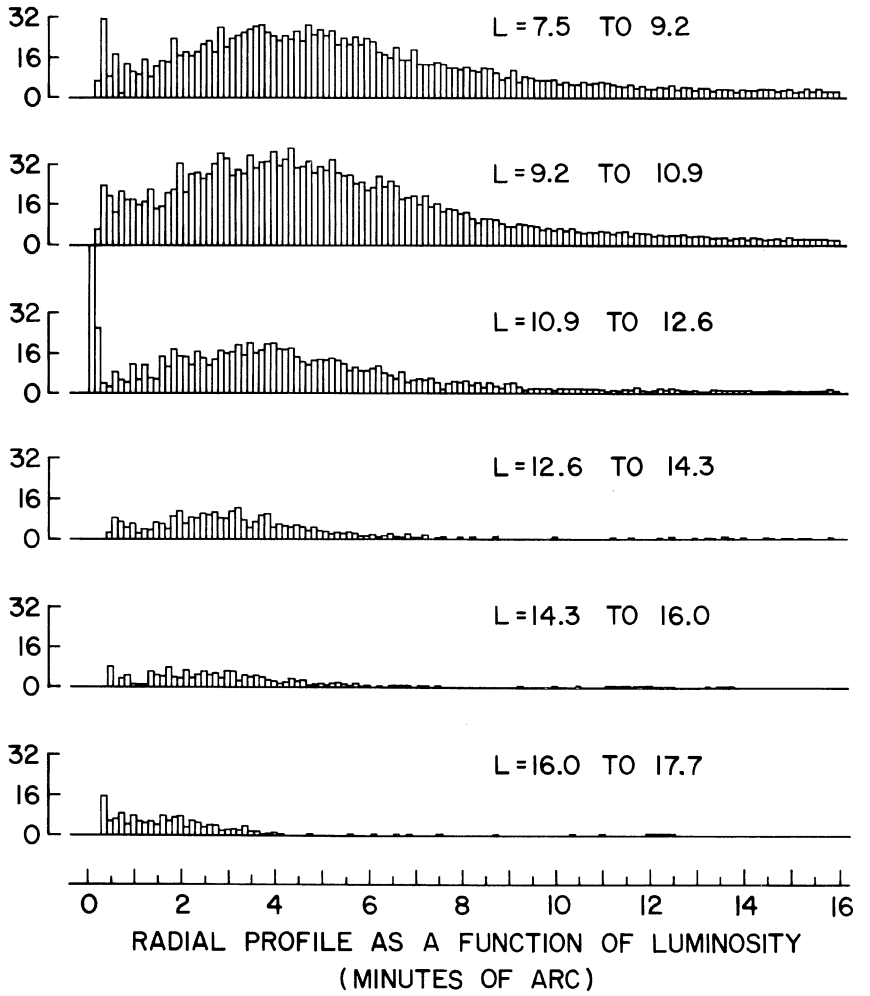

FIG. 5(b). Radial profiles as a function of star brightness. Numbers represent all images counted by the APM in radial bins of 7.″61 and brightness intervals of 1.7 APM magnitudes (faintest stars at the top). Differences among brightness intervals are largely attributable to luminosity-dependent crowding effects.

25%. Separating out any real, small, mass-segregation effects will clearly again require calibration of the luminosity dependence of the crowding corrections on plates with varying limiting magnitudes and more sophisticated algorithms for identifying and measuring images.

V. VARIABLE STARS

The standard APM software includes provision for comparing plates and identifying possible variables automatically. Crowding of images, however, made an automatic search

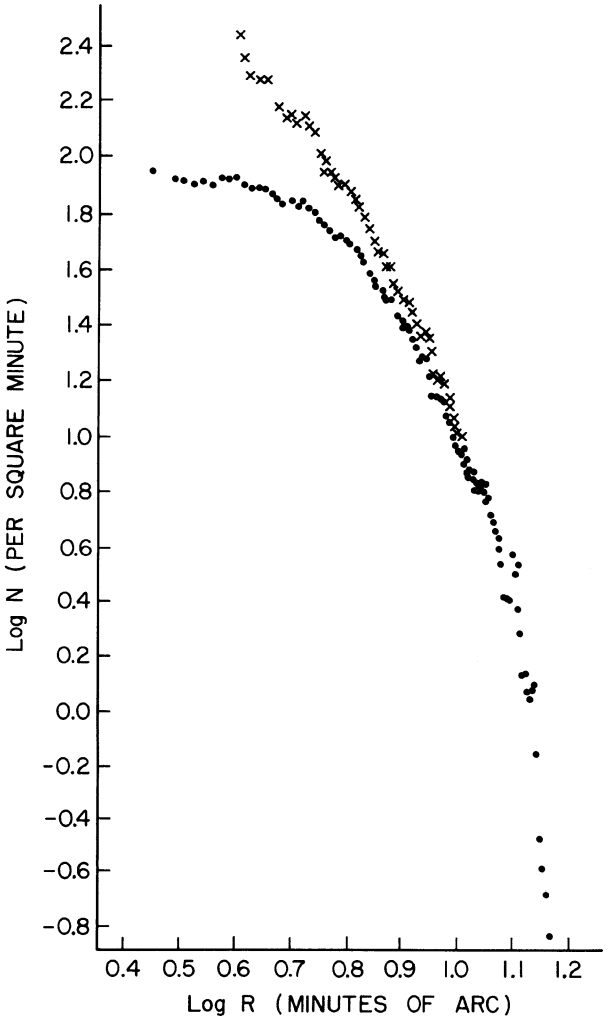

FIG. 6(a). Logarithmic radial profile for the cluster as a whole. Dots represent numbers of star images per square minute counted by the APM in 7.′61 bins, corrected for a background of 6.81 images per square minute and smoothed by taking running means of 3 bins near the center and enough bins to keep the net number of stars positive further out (5–8). ×'s are the same data corrected first for crowding in accordance with Eq. (4), then corrected for background images and smoothed. The correction algorithm clearly breaks down near 100 images per square minute, though the blip or knee just outside log $R = 0.7$ appears to be real (showing up in most subsamples and in the counts by King *et al.* 1968). The corrected data are well fit by a King (1966) model with log $R_t/R_c = 1.0$ and log $R_t = 1.3$ over the range log $R = 0.65$–1.1. The outermost points fall below the model, but could be raised back onto it by choosing a background image density about one standard deviation below our best estimate.

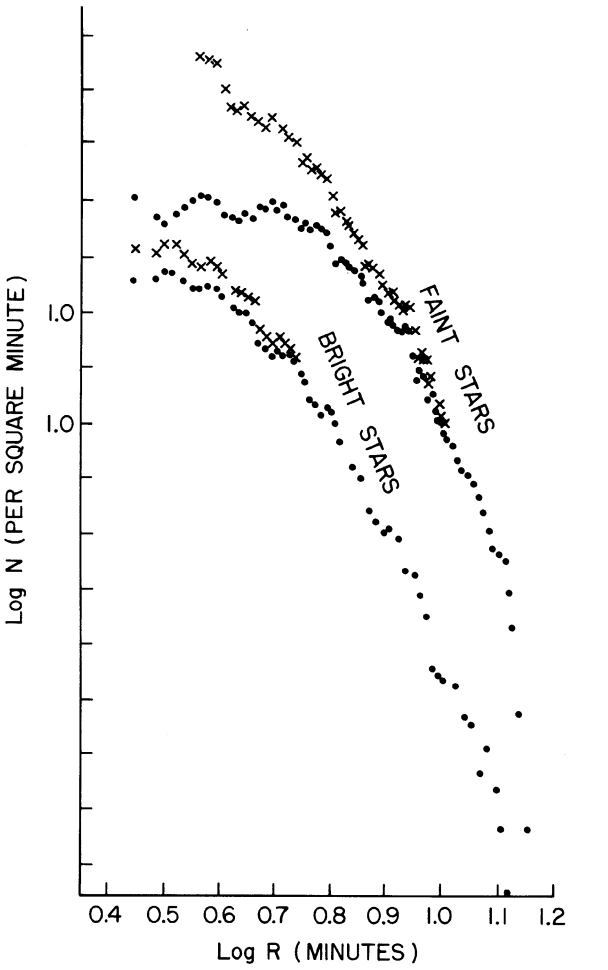

FIG. 6(b). Logarithmic radial profiles for faint ($APM \leqslant 9.2$; $M_J \geqslant 6.3$ at the cluster distance) and bright ($APM \geqslant 10.9$; $M_J \leqslant 4.7$) stars separately. Faint sample is above, and log $N = 1.0$ (10 stars per square minute) for each is indicated. Dots are data corrected for background images and smoothed by running means. ×'s were corrected first for crowding in accordance with Eq. (4). The profiles for the cluster as a whole and for these subsamples have the same shapes over the range log $R = 0.65$–1.1, where they are well fit by a King (1966) model. Nearer the center, the profiles diverge, owing to luminosity-dependent crowding effects not accounted for by Eq. (4).

for variable stars within 4′ of the cluster center unreliable. Thus the central region of each plate was additionally scanned to produce pixel intensity maps. These were digitally adjusted, pairwise, to have the same seeing profiles and intensity calibrations; and a process best described as "digital blinking" was then used to look for candidate variables. Of the six known RR Lyrae stars (King 1947; Hogg 1973; King and Bruzual 1976), two were clearly variable in the automatic mode and three probably variable in the raster scans, which also identified one additional candidate variable of about the same brightness, near the cluster center. This star is not one of those for which Alcaino (1975), Harris (1975), or Lee (1977) provided photometry, and we do not know its color or anything else about it. It is listed with the others in Table III.

We found no additional candidate variables for several magnitudes down from the RR Lyraes, but eight possible variables turned up in the range $M_J = 5$–7 in the automatic search in the outer regions of the cluster. The apparent variability is typically 0^m5, compared to a mean error per plate (cf. Table IV) of 0.03–0^m07 for $J = 18$–21. Liller (1983) has independently, and earlier, identified the first three of our

TABLE III. Known and candidate variables in M55.

ID (Alcaino 1975; King 1947)	R.A.[a]	Decl.[a]	(a) RR Lyraes M_J on plate used for counts	Comments
59 (v1)	19h 37m 12s1	−31°5′23″	0.11	Variable in automatic search
96 (v3)	19 36 54.8	−31 9 32	0.46	Variable in automatic search
366 (v2)	19 36 31.8	−31 4 54	1.31	Possibly variable in raster
433 (v4)	19 36 57.1	−31 3 30	1.26	Possibly variable in raster
456 (v6)	19 36 57.3	−31 4 48	—	No evidence for variability
592 (v5)	19 36 45.3	−31 5 42	—	Variable in raster
—	19 36 49.3	−31 4 30	1.69	Variable in raster; new candidate

R.A.[a]	Decl.[a]	(b) Fainter stars M_J on three plates scanned	Comments
19h 37m 36s3	−30°54′58″	6.56, 6.04, 6.03	Confirmed; $P = 1.3$ days
19 38 3.4	−30 55 45	5.51, 5.44, 6.07	Confirmed; $P = 0.77$ days
19 37 31.2	−31 2 49	4.94, 4.78, 4.40	Confirmed; $P \leqslant 0.2$ days?
19 37 28.8	−30 56 43	5.56, 5.50, 5.97	Variable in automatic search
19 36 21.9	−31 8 26	4.52, 5.40, 5.37	Variable in automatic search
19 37 43.6	−31 9 24	6.24, 6.08, 6.56	Variable in automatic search
19 36 57.8	−31 11 22	6.68, 7.02, 6.74	Variable in automatic search
19 37 4.5	−31 12 13	6.74, 6.49, 6.83	Variable in automatic search

[a] Relative to the PERTH 70 standard stars. The easiest way to find one's way around the cluster is probably to use the known RR Lyraes numbered in Alcaino's finding charts.

candidates as variable stars by conventional methods. From eight plates taken over three nights, she finds periods of 1.3 and 0.77 days for the first two stars and no satisfactory period longer than 0.2 days for the third. She finds the others constant to within 0.2–0m3 and reports two other faint variables (one a background RR Lyrae) which we did not pick out. We confess to being enormously encouraged to find that the APM has done even 3/8 as well as this very experienced human observer!

The number of these certain and possible variables, their brightnesses, and the amounts and time scales of their variability are consistent with their being the W UMa stars we originally set out to look for (presupposing normal, Population I, binary statistics for the cluster). S. M. Rucinski suggests that they might, alternatively, by BY Dra (spotted, rotating, flare) stars, which are occasionally found among old, high velocity, stars (e.g., CM Dra and YY Gem). Figure 7 (Plate 2) indicates their location in the cluster.

VI. CONCLUSIONS AND FUTURE PROSPECTS

We conclude that automatic plate measurement shows considerable potential for doing useful star counts, luminosity functions, and variable star searches in moderately crowded fields. Further work is needed to overcome confusion effects in crowded fields by (a) calibrating the luminosity dependence of the fraction of images missed and (b) devising an algorithm for image identification and measurement that can be used when plate coverage at threshold isophote exceeds 20%. Much smaller images (e.g., from Space Telescope) would, of course, also solve the problem.

For this particular globular cluster, we have rediscovered previously known features including the gradual flattening of the luminosity function for stars fainter than $M_J \sim 5.5$ (visible even in the outskirts of the cluster), a small blip in the radial profile near $R = 5'$, and most of the RR Lyrae stars. In addition, we have found evidence possibly for mass segregation (but more probably for brightness-dependent confusion in the automatic counts) and eight possible main-sequence variables, three of them independently confirmed. They could be W UMa or BY Dra stars at $M_J = 5$–7 and would repay further study.

APM measurement of pairs of plates taken in different colors should be capable of producing color-magnitude diagrams quickly and with good uniformity over a cluster field. An attempt to do this for M55 using existing Harvard survey plates produced not much better than a scatter diagram, owing to the short exposure times and poor image qualities on the yellow plates. We hope to be able to try this again with suitable AAT plates in due course.

TABLE IV. Errors in measured machine magnitudes as a function of apparent magnitude J. These were derived from a scatter plot of all matched intensities measured on two separate plates and represent the error per plate. The errors for bright images are larger than they would be in an uncrowded field.

J magnitude	Magnitude error
21	0.066
20	0.048
19	0.037
18	0.031
17	0.029
16	0.027
⩽15	0.027

We are deeply indebted to Drs. David Hanes and David Malin of the Anglo-Australian Observatory for obtaining the three plates used in this investigation. Without their collaboration, via the AAO's Service Photography Program, this project could never have gotten started. Equal gratitude goes to the members of the APM staff, Dr. Edward J. Kibblewhite (director), Peter S. Bunclark, and Michael T. Bridgeland for their work in developing this valuable facility and to the SERC for supporting it. We are also grateful to Prof. Ivan R. King for the suggestions which prompted this inves-

tigation and for finding charts and other practical advice and assistance, and to Harvard College Observatory and to Dr. Martha H. Liller for the use of the survey plates of M55.

Neither of us had any previous experience in globular cluster star counts, and we thus particularly appreciate the kindness of the more knowledgeable colleagues who provided comments and advice after reading the first draft of this paper. They are Drs. Gonzalo Alcaino, Gary Da Costa, Ivan King, Martha Liller, Bohdan Paczyński, and Charles Peterson, and an anonymous referee. V.T. is grateful for the usual warm hospitality of the Institute of Astronomy, Cambridge, during the period the plates were being scanned and the data reduced.

APPENDIX

Let $F(r)$ be the cumulative distribution function of the statistic r, in this case the distance between one particular star chosen at random and its surrounding neighbors. Then, given a sample of n such measures, the probability that the k th ordered value (i.e., k th nearest neighbor) be within a distance r is

$$P(r_k \leqslant r) = \sum_{j=k}^{n} {}^nC_j [F(r)]^j [1 - F(r)]^{n-j} \quad \text{(A1)}$$

(see, for example, Lindgren 1976). We can rewrite this expression in a more convenient form as

$$P(r_k \leqslant r) = 1 - \sum_{j=0}^{k-1} {}^nC_j [F(r)]^j [1 - F(r)]^{n-j}. \quad \text{(A2)}$$

The function $F(r)$, for a locally random distribution of points, simply depends on the area, πr^2, and a normalization constant α. If we assume that, to first order, stellar images are circularly symmetric and can be specified with some mean threshold isophotal radius, r_t, then the probability of finding another star within a distance $2r_t$ (that is, overlapping) is given by the nearest-neighbor distribution

$$C_1(r) = 1 - [1 - F(r)]^n, \quad \text{(A3)}$$

where we have written the distance as $r = 2r_t$ for notational simplicity. For large n, this expression can be written in the more familiar form

$$C_1(r) \simeq 1 - \exp(-\pi n \alpha r^2). \quad \text{(A4)}$$

Similarly, the probability of finding the second nearest neighbor within this distance is given by

$$C_2(r) \simeq 1 - \exp(-\pi n \alpha r^2) - \pi n \alpha r^2 \exp(-\pi n \alpha r^2). \quad \text{(A5)}$$

To generate higher order near-neighbor distributions it is simplest to use the recursion relation

$$C_j(r) = C_{j-1}(r) - {}^nC_{j-1} [F(r)]^{j-1} [1 - F(r)]^{n+1-j}.$$

Let us define the local number density of stars as f' and the measured number density as f, then

$$f = f'[(1 - C_1) + \tfrac{1}{2}(C_1 - C_2) + \cdots + (1/j)(C_{j-1} - C_j) + \cdots], \quad \text{(A7)}$$

where the first term in the brackets is the proportion counted as single stars, the second term double images, and so on. Using Eq. (A6) we can rewrite this as

$$f = f' \sum_{j=1}^{n} \frac{1}{j} {}^nC_{j-1} [F(r)]^{j-1} [1 - F(r)]^{n+1-j}. \quad \text{(A8)}$$

For large n, after some simplification this expression reduces to

$$f \simeq f' \frac{[1 - \exp(-\pi n \alpha r^2)]}{\pi n \alpha r^2}. \quad \text{(A9)}$$

Now $n\alpha$ is just the mean number density of stars, f', and $\pi r^2 = 4\pi r_t^2 = 4A'$, where A' is the area of a single star image at threshold isophote. Therefore, the correction formula for crowding reduces to the simple expression

$$f \simeq f' \frac{[1 - \exp(-4f'A')]}{4f'A'}, \quad \text{(A10)}$$

which can be rewritten in terms of the unknown f' as

$$f'A' \simeq -\tfrac{1}{4} \ln(1 - 4fA'). \quad \text{(A11)}$$

REFERENCES

Alcaino, G. (1975). Astron. Astrophys. Suppl. **22**, 193.
Alcaino, G. (1977). Astron. Astrophys. Suppl. **29**, 383.
Bahcall, N. (1977). Annu. Rev. Astron. Astrophys. **15**, 505.
Bahcall, J., and Soneira, R. (1981). Astrophys. J. Suppl. **47**, 357.
Bok, B. (1977). Publ. Astron. Soc. Pac. **89**, 597.
Bunclark, P. S., and Irwin, M. J. (1983). In *Statistical Methods in Astronomy*, ESA Spec. Publ. SP-201 (in press).
Da Costa, G. (1982). Astron. J. **87**, 990.
Da Costa, G., and Freeman, K. C. (1976). Astrophys. J. **206**, 128.
Harris, W. E. (1975). Astrophys. J. Suppl. **29**, 397.
Harris, W. E., and Racine, R. (1979). Annu. Rev. Astron. Astrophys. **17**, 241.
Herschel, W. (1785). Philos. Trans. R. Soc. **75**, 213.
Herzog, A. D., and Illingworth, G. D. (1977). Astrophys. J. Suppl. **33**, 55.
Hogg, H. S. (1973). Publ. David Dunlap Obs. **3**, No. 6.
Hoskin, M. A. (1982). *Stellar Astronomy* (Science History Publications, Chalfont St. Giles), p. 71.
Kibblewhite, E. J., Bridgeland, M. T., Bunclark, P., and Irwin, M. (1983). In *Proceedings of the Astronomical Microdensitometry Conference (AMC)* (to be published).
King, I. R. (1947). Harvard Obs. Bull. No. 920.
King, I. R. (1966). Astron. J. **71**, 64.
King, I. R. (1975). In *Dynamics of Stellar Systems*, IAU Symposium No. 69, edited by A. Hayli (Reidel, Dordrecht), p. 99.
King, I. R. (1983). Private communication.
King, I. R., and Bruzual, G. (1976). Astron. Astrophys. **50**, 459.

King. I. R., Hedemann, E., Jr., Hodge, S. M., and White, R. E. (1968). Astron. J. **73**, 456.
Lee, S.-W. (1977). Astron. Astrophys. Suppl. **29**, 1.
Liller, M. H. (1983). Private communication.
Lindgren, B. W. (1976). *Statistical Theory* (Macmillan, New York), p. 218.
Newell, E. B. (1979). In *Image Processing in Astronomy*, edited by G. Sedmek, M. Capaccioli, and R. J. Allen (Observatorio Astronomico, Trieste), p. 100.
Newton, I. (1692). Unpublished draft of Prop. XV, Theor. XV, for 2nd edition of *Principia*, in University Library Cambridge, Add. MS 3965, folios 275 recto, 275 verso, 276^{r}, 185^{r}, 184^{v}. Cited by Hoskin (1982).
Paczyński, B. (1983). Private communication.
Peterson, C. J. (1976). Astron. J. **81**, 617.
Peterson, C. J., and King, I. R. (1975). Astron. J. **80**, 427.
Simoda, M., and Tanikawa, K. (1972). Publ. Astron. Soc. Jpn. **24**, 1.
Tomita, Y., Saito, T., and Ohtani, H. (1979). Publ. Astron. Soc. Jpn. **31**, 407.
Trimble, V. (1977). Astrophys. Lett. **18**, 145.
Trimble, V. (1980). In *Star Clusters*, IAU Symposium No. 85, edited by J. Hesser (Reidel, Dordrecht), p. 259.
de Vaucouleurs, G. (1948). Ann. Astrophys. **11**, 247.
Webbink, R. (1980). In *Close Binary Stars*, IAU Symposium No. 88, edited by M. Plavec, D. Popper, and R. Ulrich (Reidel, Dordrecht), p. 561.
Weistrop, D. (1968). Private communication.

PLATE 2

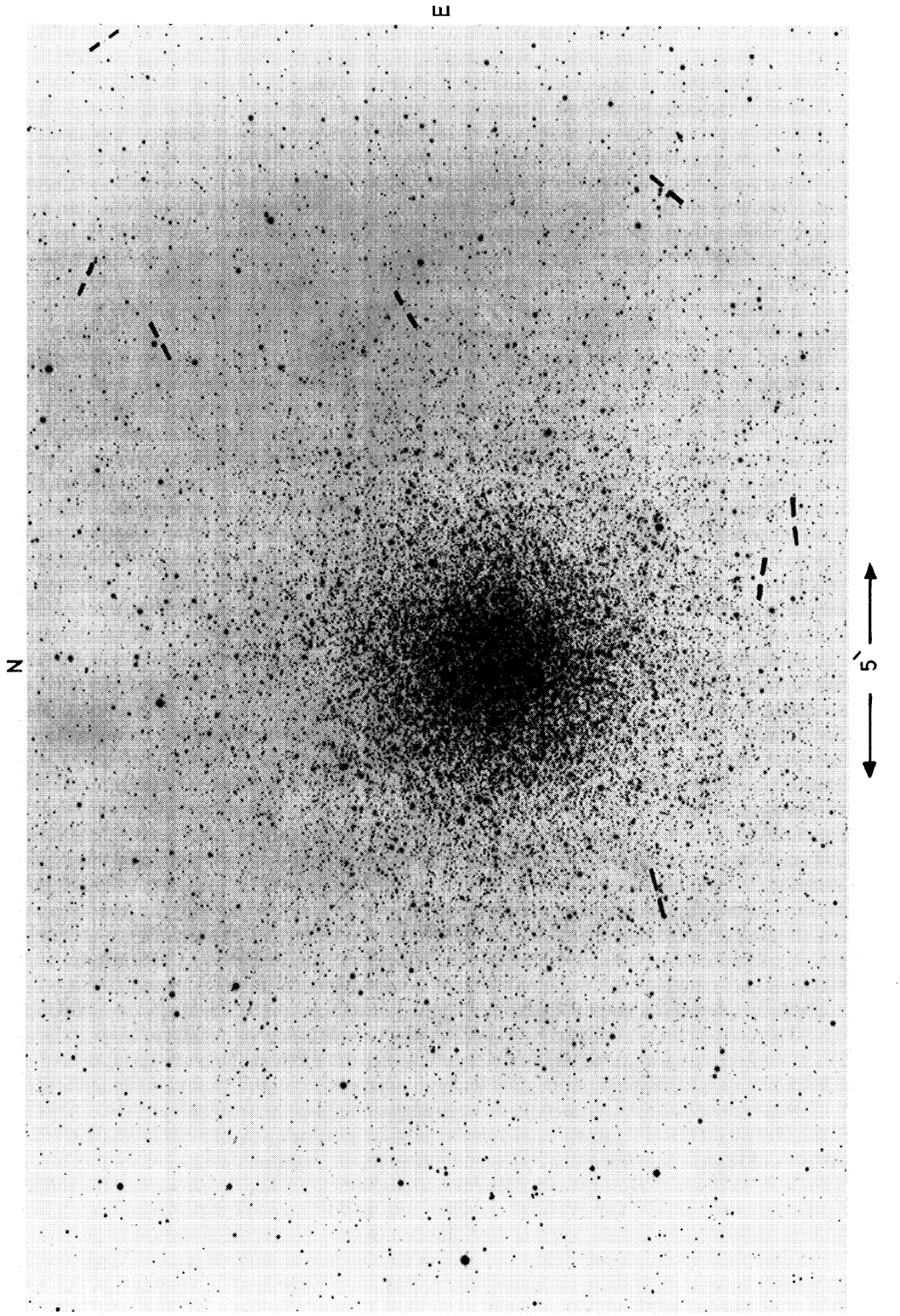

FIG. 7. Reproduction of AAT photograph of M55 showing locations of faint variable candidates.

Michael J. Irwin and Virginia Trimble (see page 92)